Interactions Between Turbulent Wakes and Boundary Layers

D. Agoropoulos* and L. C. Squire†
Cambridge University, Cambridge, England, United Kingdom

Experimental measurements and numerical computations are presented for five cases of two-dimensional turbulent wakes mixing with boundary layers. These were set up so as to simulate the positive streamwise pressure gradient and wake structure found on multi-element aerofoils. The algebraic stress turbulence model of Rodi, in conjunction with the boundary-layer equations, successfully postdicted all five test cases, outperforming an improved version of the k-ε model. A minor failure of both methods to postdict accurately the edge of the wake may be attributed to its intermittency.

I. Introduction

IN the flow over high-lift multi-element aerofoils, the wakes of upstream elements flow over and mix with the boundary layers of downstream elements. This wake/boundary-layer interaction has been identified as a problem of special interest for the development of calculation methods to predict accurately the viscous flow over such a wing.

A few studies[1-3] on fairly realistic aerofoil configurations have been recently reported. However, the complexity of the flow is such that it is impossible to identify the effects associated with the various parameters of the aerofoil/slat system, yet these effects must be understood if a reliable prediction method is to be developed. Work aimed at gaining this understanding was begun in the Cambridge University Engineering Department with the work of Zhou and Squire.[4, 5] The current project was conceived in order to extend their measurements, as well as calculations, into more realistic wake/boundary-layer merging flows. It was decided to concentrate on the interaction between the wake of the slat and the boundary layer on the main wing element since it is normally stronger than that between the main element wake and the boundary layer on the flap for a typical three-element aerofoil. At all times, the emphasis was placed on the careful and thorough comparison of experiment and theory by looking at a few well-defined test cases representative of high-lift aerofoils.

The objectives can be summarized as follows: 1) to set up a realistic flow around the slatted nose of a high-lift two-dimensional aerofoil, 2) to model the main features of this flow in a large-scale boundary-layer tunnel and obtain detailed measurements of the mean and turbulent flowfields, and 3) to calculate the aforementioned flow using second-order turbulence models.

II. Experimental Work

To achieve the first objective, a circulation control model (CCM) was designed and tested. It consisted of an elliptic main element together with a realistic sharp-heeled slat (Fig. 1), fitted with end plates so as to increase the effective aspect ratio and ensure satisfactory two-dimensional flow conditions (Fig. 2). High-lift coefficients were achieved by means of tangential blowing into the upper-surface boundary layer near the trailing edge of the ellipse.[6] The nose geometry was varied by adjusting the position of the slat relative to the main elliptic element. Several geometrical configurations were tried at different blowing rates until a satisfactory leading-edge flow with a realistically high suction peak of $C_p = -5$ was achieved. This suction peak may be seen in Fig. 3 to correspond to configuration 2. Measurements were limited to surface static pressure distribution on the ellipse and some total pitot traverses in the confluent viscous flow of the slat wake and ellipse boundary layer to confirm their interactive nature (these results are not shown here). The Reynolds number based on the slat chord was 300,000 and thus was very similar to that of other recent experiments on multi-element aerofoils.[7, 8]

In the second stage, the main features of the CCM merging flow were transferred into the large-scale boundary-layer tunnel (blower) of Zhou and Squire[4, 5] shown in Fig. 4. The pressure gradient was matched between the two flows by means of the following viscous pressure-gradient parameter (Fig. 5):

$$\delta^* \frac{dC_p^*}{dx}$$

where δ^* = displacement thickness of wall layer at $x = 0$ (trailing edge of slat) and $C_p = (p - p_\infty)/\frac{1}{2}\rho U_{\text{ref}}^2$, a static pressure coefficient based on the inviscid velocity at the trailing edge of the wake-generating model as obtained from the corresponding wall static hole. It should be noted that because the slat Reynolds number was virtually identical between the circulation control model and the blower tunnel flows, the particular choice of δ^* as a suitable length scale is not critical.

The separation bubble that occurs downstream of the heel on the lower surface of the slat was also modeled. Two models were used: model 1 (set 1) was the thick (38%), sharp-edged model B of Zhou and Squire, whereas model 2 (sets 2, 3, 4, and 5) was a thin (15%) model used both with and without a leading-edge fence to create a separation bubble on the wall side. Two different streamwise pressure distributions were es-

Config.	α_s (°)	h (mm)	Overlap	Measurements
1	15.0	14.5	0	pressures
2	21.3	14.5	0	ditto
3	10.5	14.5	0	ditto
4	21.0	7.8	0	ditto
5	21.0	10.5	0	ditto
6	21.2	14.7	0	pressures, pitot traverses

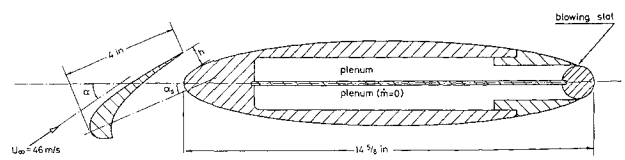

Fig. 1 Details of section of circulation control model.

Received Oct. 24, 1986; revision received July 22, 1987.

*Research Student, Engineering Department. Member AIAA.
†Reader in Engineering, Engineering Department. Associate Fellow AIAA.

tablished: one at nominally zero (sets 1 and 2) and one at positive pressure gradient (sets 3, 4, and 5) as scaled from the CCM using the aforementioned viscous pressure-gradient parameter. Set 4 corresponded to a large separation bubble, whereas set 5 did so to a small one.

In this way, well-controlled but fairly realistic merging flows were established free from the complicating effects of streamwise curvature. Moreover, the main shortcomings of the Zhou and Squire experiments were overcome; that is, the adverse pressure gradient was applied too late in their case to have any effect on the mixing, and their flow was also dominated by the severe vortex shedding from their thick model.

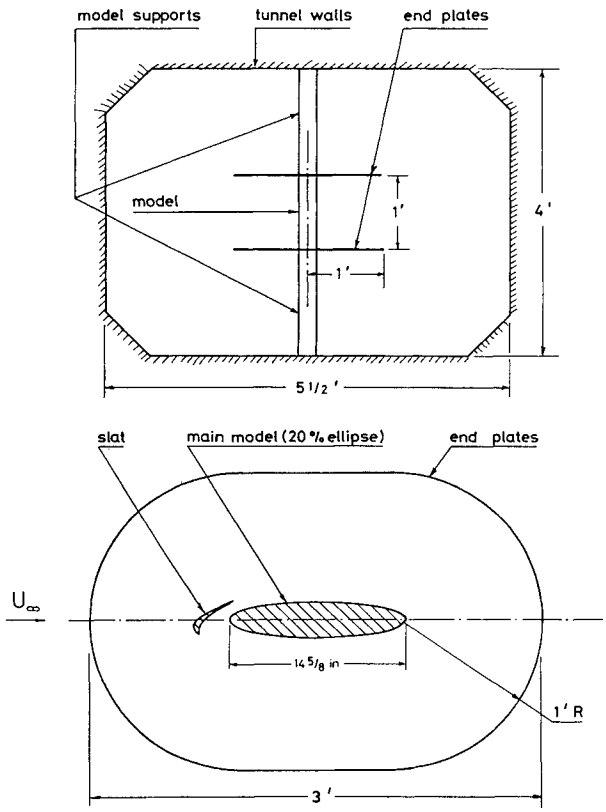

Fig. 2 Circulation control model arrangement in tunnel.

Measurements of mean velocity components U, V and Reynolds stresses $\bar{u}^2$, $\bar{v}^2$, and $-\overline{uv}$ were obtained by means of hot-wire anemometers. Disa P61 X-wire probes were used, and the signals were linearized, filtered, digitized, and processed by computer. The accuracy of the results is discussed in Ref. 9 where comparisons with pitot tube and single hot-wire traverses are also presented. The error in the mean velocity U was shown not to exceed 3% in the worst case, whereas the error in the shear stress $-\overline{uv}$ was estimated at around 7% of its maximum value; corresponding values for the normal stresses $\bar{u}^2$ and $\bar{v}^2$ were 4% and 5% of their respective local values.

Set 1 was essentially a repeat of Zhou and Squire's case e; that is, it comprises a thick-model wake with strong periodic wake shedding. The turbulence intensity is high and there is rapid mixing. Even so, recovery toward an ordinary boundary layer is rather slow, and the wake is still distinguishable at the last station, particularly if the profiles are plotted in semilogarithmic form.

When a thin model was substituted in set 2, the vortex shedding was almost eliminated, and the turbulence level in the wake fell. This produced a slower mixing so that the velocity minimum is still clearly visible at the last station (Fig. 6). The effects of the adverse pressure gradient can be assessed by comparing profiles for sets 2 and 3. Basically, the merging of the wake and the boundary layer is delayed for two reasons. First, the wake momentum thickness tends to grow under the influence of the retarding pressure force. Second, the falling velocity causes the streamlines to diverge, thereby forcing the wake centerline away from the surface. This reduces the transverse gradients and, hence, the mixing. This explanation is consistent with the observation that, even though the turbulent stresses normalized with the local freestream velocity U_e are higher in the adverse pressure-gradient case than in the constant pressure flow, the same stress when normalized by the local wake defect velocities U_o and U_i are actually lower and continuously decrease with downstream distance.

Sets 4 and 5 demonstrate the effect of the slat separation bubble, with set 4 corresponding to the larger bubble. In fact, in set 4 the bubble is so large and the inner half-wake so thick that merging has started at the first measuring station. However, the inner half-wake is not as large as in the realistic CCM model where the ratio of the inner to outer half-wake thickness

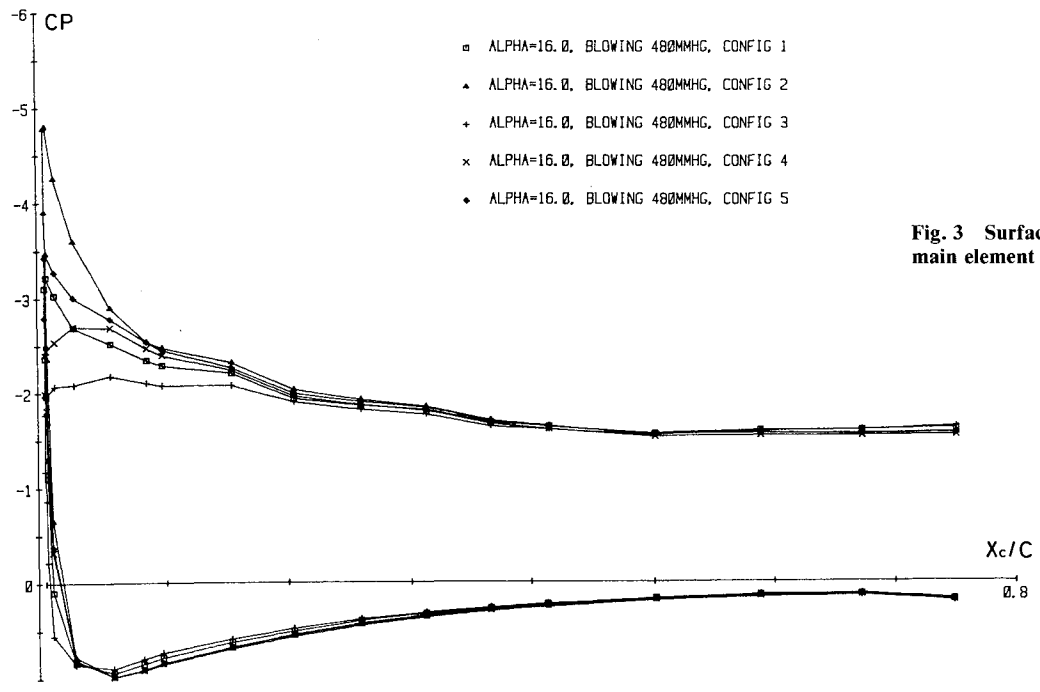

Fig. 3 Surface static pressures on the elliptic main element of the circulation control model.

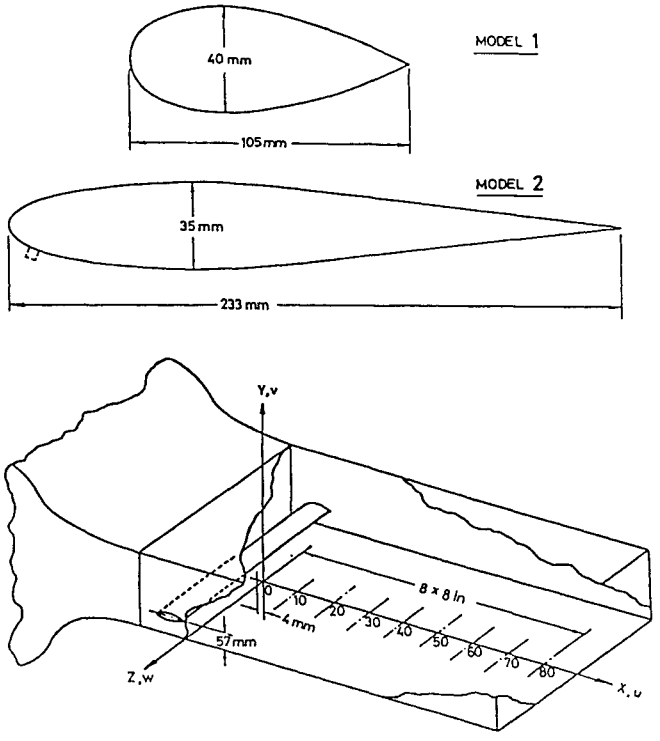

Fig. 4 Model profiles and measuring stations in the blower tunnel (model 1).

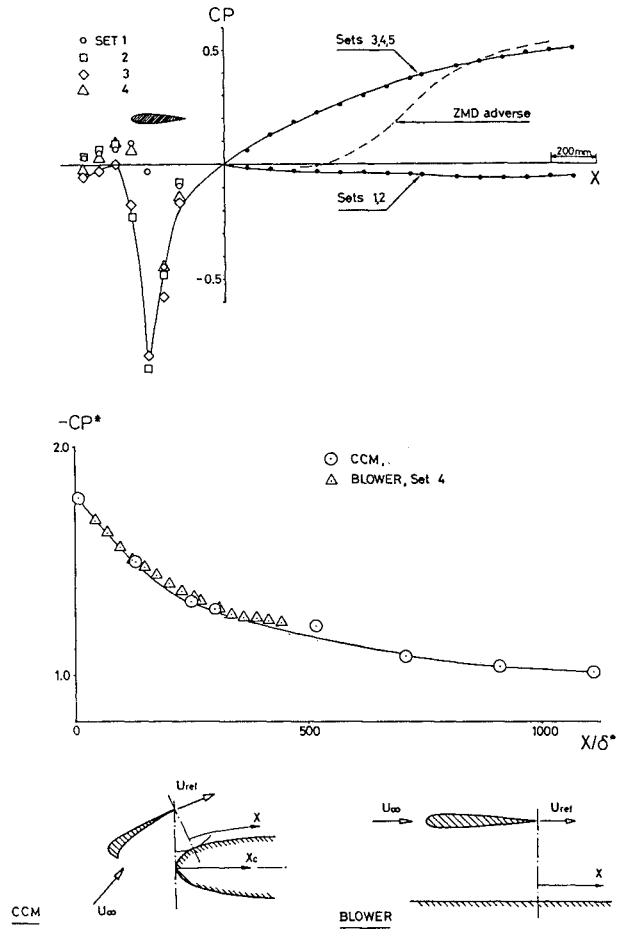

Fig. 5 Analogy between pressure distributions on the circulation control model and in the blower tunnel.

was 4, compared to only 1.6 for set 4. As well as being thicker, the turbulent intensities are considerably greater in the inner half-wake than in the outer half-wake (see Fig. 9). Consequently, mixing with the boundary layer is enhanced, the velocity minimum disappears fairly quickly, and the wake momentum deficit diffuses toward the wall, causing the confluent wake to thicken and approach separation.

In all cases, the inner half-wake is absorbed by the outer part of the boundary layer and the velocity minimum eventually disappears. However, there is very little mixing between the inner and outer half-wakes, and the development of the outer half-wake remains unaffected by the different inner half-wakes of sets 3, 4, and 5. As far as the inner half-wake is concerned, Fig. 7 confirms the existence of wall similarity for $y^+ < 200$, even in the case of the strongest interaction (set 4). It should be noted that the straight line plotted in Fig. 7 corresponds to a semilogarithmic law with the same constants as for ordinary boundary layers. This fact was exploited to advantage by adopting universal wall functions in the subsequent numerical computations.

III. Numerical Work

Integral methods have proved unsuccessful and very restrictive in attempts to calculate wake/boundary-layer interacting flows in the past.[10] The advent of finite-difference methods[11] has effected a greater flexibility, but the need for a turbulence model more sophisticated than the commonly employed mixing length has been identified. One would ideally like to be able to predict regions of negative eddy viscosity such as those occurring in strong interactions.[4,5] However, these regions tend to be small in practice and they were barely detectable in the present sets 2–5.

A. Governing Equations

In the present work, the thin shear-layer approximations to the Navier-Stokes equations were solved in conjunction with two different turbulence models: k-ε and the algebraic stress model (ASM) of Rodi. The program consists of an enhanced version of the PASSABLE code, originally developed for the 1980–81 Stanford conference.[12] The basic equations are as follows:

$$\frac{\partial U}{\partial x} + \frac{\partial V}{\partial y} = 0 \tag{1}$$

X momentum:

$$U\frac{\partial U}{\partial x} + V\frac{\partial U}{\partial y} = U_e\frac{\mathrm{d}U_e}{\mathrm{d}x} + \frac{1}{\rho}\frac{\partial \tau_{xy}}{\partial y} \tag{2}$$

where $\tau_{xy} = \mu\partial U/\partial y - \rho\overline{uv}$ is the shear stress.

$$\frac{\partial k}{\partial t} + U_i\frac{\partial k}{\partial x_i} = T_k - \overline{u_iu_j}\frac{\partial U_i}{\partial x_j} - \varepsilon \tag{3}$$

$$\frac{\partial \varepsilon}{\partial t} + U_i\frac{\partial \varepsilon}{\partial x_i} = T_\varepsilon + C_{\varepsilon 1}\frac{\varepsilon}{k}P_k - C_{\varepsilon 2}\frac{\varepsilon^2}{k} - C_{\varepsilon 3}\frac{\varepsilon}{k}\frac{\partial U}{\partial x}(\overline{u^2} - \overline{v^2}) \tag{4}$$

The Reynolds stresses $\overline{u_iu_j}$ and the turbulent transport (diffusion) terms T_k and T_ε are modeled as follows:

k-ε model:

$$-\overline{u_iu_j} + \frac{2}{3}k\delta_{ij} = \nu_T\left(\frac{\partial U_i}{\partial x_j} + \frac{\partial U_j}{\partial x_i}\right) \tag{5}$$

$$\nu_T = C_\mu k^2/\varepsilon \tag{6}$$

$$T_k = \frac{\partial}{\partial y}\left(\frac{\nu_T}{\sigma_k}\frac{\partial k}{\partial y}\right) \tag{7}$$

$$T_\varepsilon = \frac{\partial}{\partial y}\left(\frac{\nu_T}{\sigma_\varepsilon}\frac{\partial \varepsilon}{\partial y}\right) \tag{8}$$

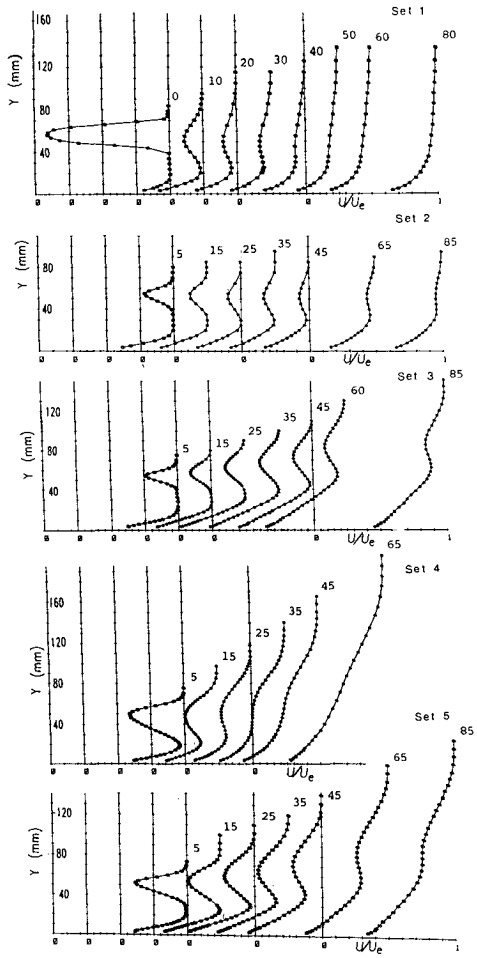

Fig. 6 U/U_e profiles measured in the blower tunnel.

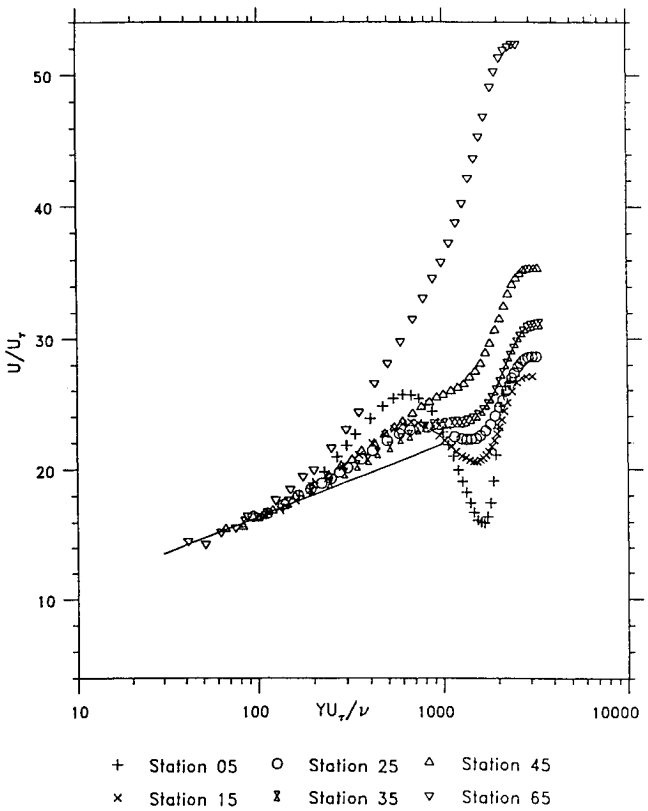

Fig. 7 Law-of-the-wall profiles: set 4.

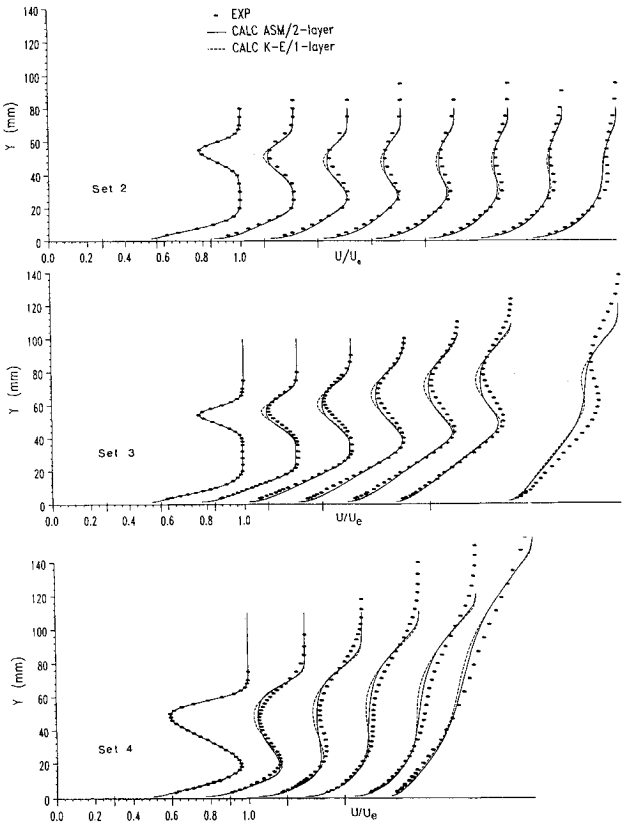

Fig. 8 Comparison of calculated and measured U/U_e profiles, sets 2, 3, and 4.

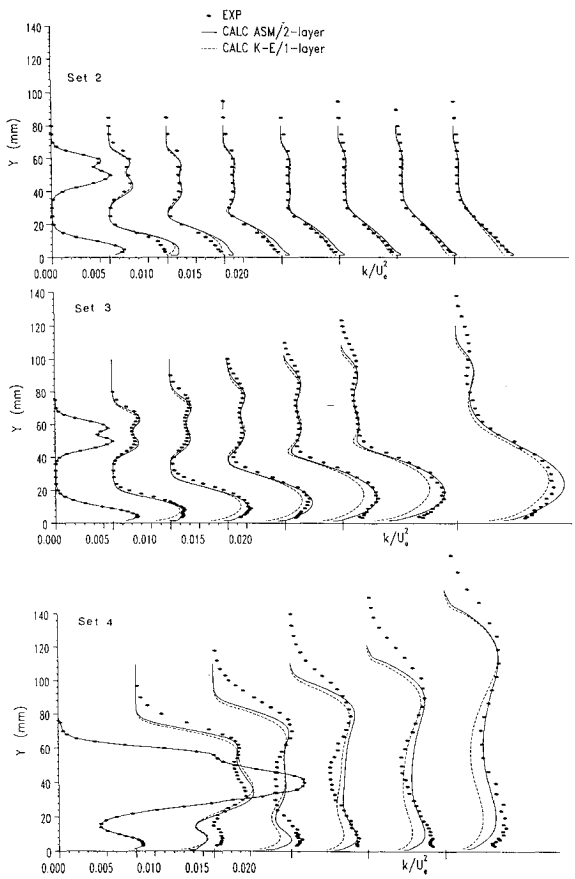

Fig. 9 Comparison of calculated and measured k/U_e^2 profiles, sets 2, 3, and 4.

ASM:

$$\frac{\overline{u_i u_j}}{k}(P_k - \varepsilon) = P_{ij} + \phi_{ij} - \frac{2}{3}\varepsilon\delta_{ij} \tag{9}$$

$$T_k = C_s \frac{\partial}{\partial y}\left(\frac{k}{\varepsilon}\overline{v^2}\frac{\partial k}{\partial y}\right) \tag{10}$$

$$T_\varepsilon = C_\varepsilon \frac{\partial}{\partial y}\left(\frac{k}{\varepsilon}\overline{v^2}\frac{\partial \varepsilon}{\partial y}\right) \tag{11}$$

where ϕ_{ij} represents the pressure-strain term and $P_k = \frac{1}{2}P_{ii}$ is the production rate of the turbulent kinetic energy k.

As part of the present work, the original PASSABLE code has been extended to account for the effects of small departures from exact two-dimensionality that commonly affect nominally two-dimensional flows, as well as for the second-order terms due to normal stresses and transverse pressure gradient $\partial p/\partial y$ in Eq. (2). The former correction adds a term $\partial W/\partial z = DU$ to the left-hand side of the continuity equation, Eq. (1), on the assumption that the velocity profiles are collinear so that the divergence D may be taken as constant through the shear layer.[13] Second-order corrections to the x-momentum equation have been considered by various workers, e.g., Johnston,[14] and for plane flows they normally involve the addition of an extra term $-\partial(u^2 - v^2)/\partial x$ to the right-hand side of Eq. (2).

In the area of turbulence modeling, the main extension involved sensitizing the ε equation to irrotational strains via the last term on the right-hand side of Eq. (4) after Hanjalic and Launder.[15] Following their proposal, $(\overline{u^2} - \overline{v^2})$ was approximated by 0.33 k in the case of the k-ε model, which, of course, does not solve for the individual Reynolds stresses. Wall functions were employed near the wall,[16] and the standard values of all the constants were used as given in Ref. 12, except for $C_\varepsilon = 0.173$ and $C_{\varepsilon 3} = 2.5$ as recommended in Refs. 14 and 17.

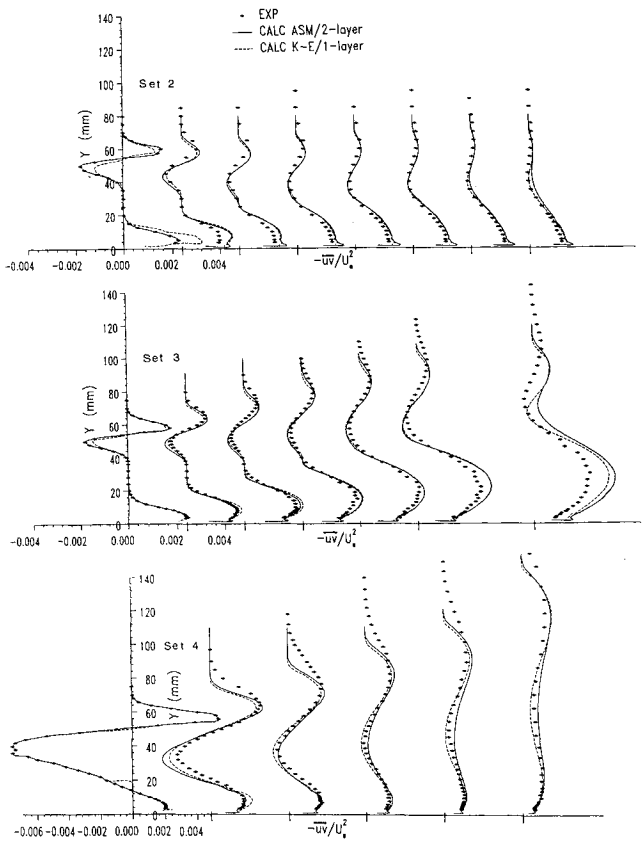

Fig. 10 Comparison of calculated and measured $-\overline{uv}/U_e^2$ profiles, sets 2, 3, and 4.

The calculation was started using the experimental profiles of U and turbulent kinetic energy at the first station. Initial profiles of ε were prescribed from

$$\varepsilon = C_\mu \frac{k^2}{\nu_T} \tag{12}$$

on the basis of measured values of k and eddy viscosity ν_T, even though the forward-marching solution was not very sensitive to a difference of, say, 20% in the initial ε profile. Values of the divergence $D = D(x)$ were provided from the out-of-balance term in the two-dimensional momentum integral equation as applied to the measured profiles.[9]

B. Results

Postdictions of Zhou and Squire's set e,[4] which was virtually identical to set 1, using similar second-order closures have been previously reported[18,19] and thus will not be presented here. Also, because set 5 was similar to set 4 but had a smaller separation bubble on the slat model, results will only be given here for the more severe latter case.

In Fig. 8, profiles of computed U velocity are compared with experimental measurements, whereas turbulent kinetic energy and shear-stress profiles are similarly presented in Figs. 9 and 10, respectively. Figure 11 shows the individual Reynolds stresses $\overline{u^2}/U_e^2$ and $\overline{v^2}/U_e^2$ for set 4. The agreement between theory and experiment is good, particularly so for the Reynolds stresses with the ASM model. The calculated mean velocity profiles have the correct shape but tend to be underpostdicted toward the downstream end. Because the divergence D is not necessarily constant (collinear) through the complex confluent layer, the correction is only approximate at the downstream end of the tunnel, where tunnel-exit effects also become important. Nevertheless, Figs. 9–11 demonstrate that the extra rates of strain are too small to affect the Reynolds stresses.

Along the centerline of the wake, where the difference between production and dissipation of k is large and increases under flow deceleration, the ASM predicts the mean velocity U more accurately than the k-ε model. This is because whereas C_μ is constant for the k-ε, the same parameter effectively becomes a function of P_k and ε under the ASM.

The profiles corresponding mainly to set 4 in Figs. 8–11 indicate a failure to postdict the edges of the wake correctly.

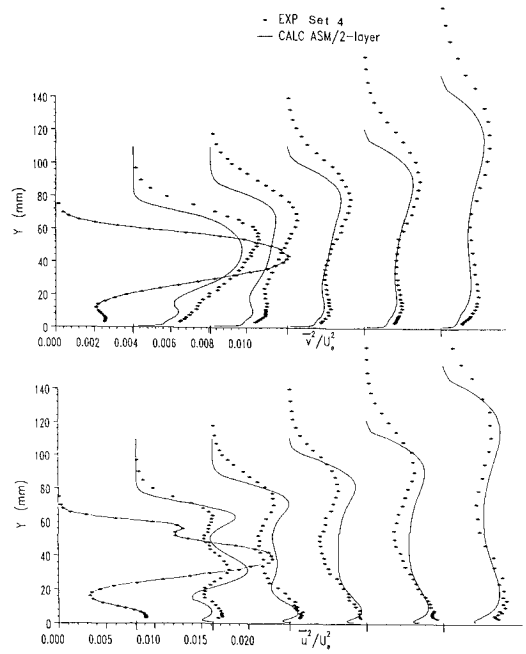

Fig. 11 Comparison of calculated and measured $\bar{u}^2/U_e^2$ and $\bar{v}^2/U_e^2$ profiles, set 4.

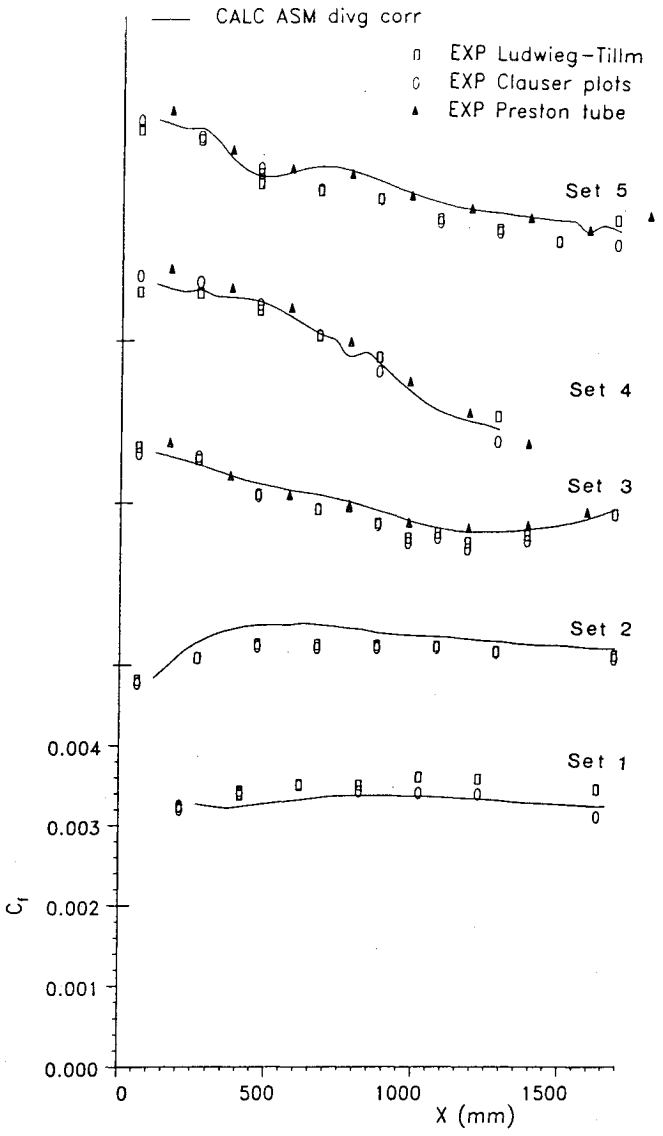

Fig. 12 Comparison of calculated and measured skin-friction coefficients.

The calculated wake appears to be approaching the freestream, as well as the boundary layer along the inner edge, too sharply during the initial stages of the merging. Such a phenomenon, which has also been observed in calculations of wakes using the k-ε model, may be explained in terms of the marked intermittency that characterizes the turbulent motion of wakes.[20] The Reynolds stresses illustrate this behavior to be true for both the k-ε and ASM models (Figs. 9–11). This is hardly surprising given the use of closures based on time-averaged, fully turbulent flows. Improvement could in principle be effected by prescribing a suitable intermittency distribution $\gamma[=\gamma(y)]$ to correct the eddy viscosity to

$$\nu_T = \frac{C_\mu}{\gamma}\frac{k^2}{\varepsilon} \tag{13}$$

Such a correction was successfully employed by Patel and Scheuerer[20] in far wakes. In our case, however, this would not seem worthwhile since the wake quickly "fills up" during the subsequent stages of the merging.

As a final result, skin-friction coefficient and momentum thickness distributions are plotted in Figs. 12 and 13, respectively. The comparison with the experimental is favorable, particularly for the skin-friction postdictions under adverse pressure-gradient conditions.

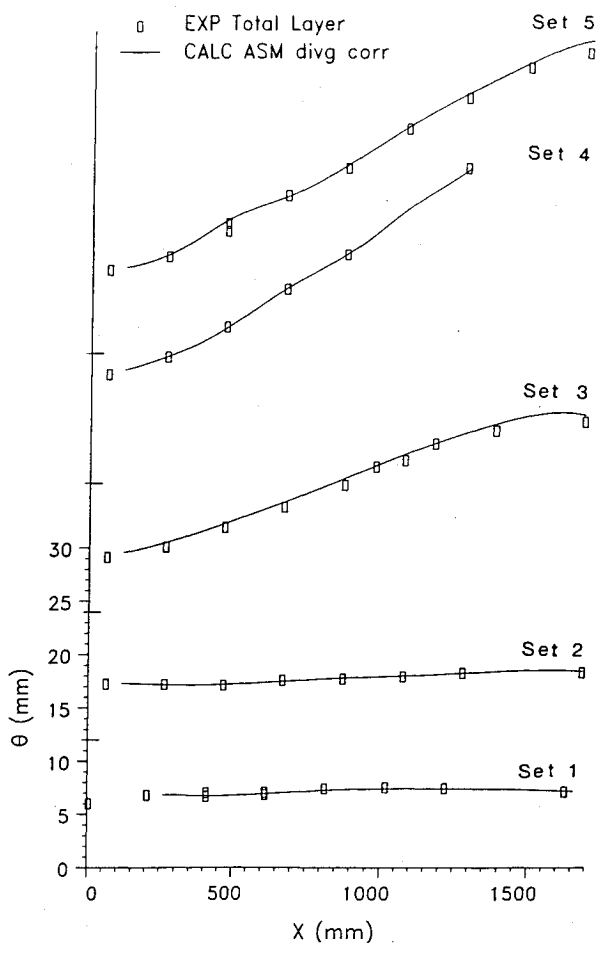

Fig. 13 Comparison of calculated and measured momentum thicknesses.

IV. Conclusions

It is thus believed that the objectives of this project have been substantially achieved. Substituting a thin (15%) for a thick (38%) wake-generating model eliminated vortex shedding and suppressed the phenomena of energy reversal and high $\bar{v}^2$ levels observed in Refs. 4 and 5. The separation bubble on a realistic slat resulted in asymmetric wake profiles and turbulence structure and promoted rapid mixing with the boundary layer. Second-order turbulence closures postdicted the main features of the flow accurately with no empirical adjustments. In particular, the all important initial stages of the merging[5] were modeled successfully, and the decelerated flows were postdicted with just the same accuracy as those in constant pressure. The ASM model proved superior to the k-ε model, while the intermittency of the wake appears not to be critical. The successful postdiction of the Reynolds shear stresses indicated that accurate prediction of the mean velocity profiles should be possible under exactly two-dimensional conditions.

References

[1]Bario, F., Charnay, G., and Papailiou, K. D., "An Experiment Concerning the Confluence of a Wake and a Boundary Layer," *Journal of Fluids Engineering*, Vol. 104, No. 1, March 1982, pp. 18–24.

[2]Brune, G. W. and Sikavi, D. A., "Experimental Investigation of the Confluent Boundary Layer of a Multielement Low Speed Aerofoil," AIAA Paper 83-0566, Jan. 1983.

[3]Braden, J. A., Whipkey, R. R., Jones, G. S., and Lilley, D. E., "Experimental Study of the Separating Confluent Boundary-Layer," NASA CR-3655, 1983.

[4]Zhou, M. D. and Squire, L. C., "The Interaction of a Wake with a Boundary Layer," Cambridge Univ., Cambridge, England, Data Rept. CUED/A-Aero/TR.11, 1982.

[5]Zhou, M. D. and Squire, L. C., "The Interaction of a Wake with a Turbulent Boundary Layer," *Aeronautical Journal*, Vol. 89, Feb. 1985, pp. 72–81.

[6]Kind, R. J., "A Proposed Method of Circulation Control," Ph.D. Dissertation, Cambridge Univ., Cambridge, England, 1967.

[7]Johnston, L. J., "Two-Dimensional Turbulent Wake/Boundary-Layer Mixing—Part 2: A Wing/Leading-Edge Slat Configuration", Queen Mary College, London, England, Paper QMC-EP-1071, 1985.

[8]Porcheron, B. and Thibert, J. J., "Etude Detaillee de l'Ecoulement autour d'un Profil Hypersustente: Comparisons avec les Calculs," AGARD CP-365, Paper 4, 1984.

[9]Agoropoulos, D., "Interactions Between Wakes and Boundary Layers," Ph.D. Dissertation, Cambridge Univ., Cambridge, England, 1986.

[10]Irwin, H. P. A. H., "A Calculation Method for the Two-Dimensional Turbulent Flow over a Slotted Flap," British Aeronautical Research Council, ARC CP-1267, 1972.

[11]Dvorak, F. A., "Calculation of Turbulent Boundary Layers and Wall Jets over Curved Surfaces," *AIAA Journal*, Vol. 11, April 1973, pp. 517–524.

[12]Launder, B. E., Leschziner, M. A., and Sindir, M., "Comparison of Computation with Experiment," *Proceedings, 1980–81, AFOSR-HTMM-Stanford Conference on Complex Turbulent Flows*, Stanford Univ., Stanford, CA, 1982, pp. 1390–1407.

[13]Head, M. R. and Prahlad, T. S., "The Boundary Layer on a Plane of Symmetry," *Aeronautical Quarterly*, Vol. 25, Nov. 1974, pp. 293–304.

[14]Johnston, L. J., "A Method to Calculate General Two-Dimensional Wall Bounded Viscous Flows," Aircraft Research Assoc., Bedford, England, Rept. 62, 1984.

[15]Hanjalic, K. and Launder, B. E., "Sensitizing the Dissipation Equation to Irrotational Strains," *Journal of Fluids Engineering*, Vol. 102, No. 1, March 1980, pp. 34–40.

[16]Launder, B. E., "Turbulence Modeling in the Vicinity of a Wall," *Proceedings, 1980–81, AFOSR-HTMM-Stanford Conference on Complex Turbulent Flows*, Stanford Univ., Stanford, CA, 1982, pp. 691–699.

[17]Rodi, W. and Scheuerer, G., "Scrutinizing the k-ε Model Under Adverse Pressure Gradient Conditions," 4th Symp. Turbulent Shear Flows, Karlsrule, FDR, Sept. 1983.

[18]Johnston, L. J., "Calculation of Wake/Boundary Layer Mixing Flows Using a Two-Equation Turbulence Model," Aircraft Research Assoc., Bedford, England, Memo 258, 1985.

[19]Nemouchi, Z., "Numerical Computation of Merging Turbulent Wakes and Boundary Layers," Univ. of Manchester Inst. of Science and Technology, Mechanical Engineering Dept., Manchester, England, Rept. TFD/83/8, 1985.

[20]Patel, V. C. and Scheuerer, G., "Calculation of Two-Dimensional Near and Far Wakes," *AIAA Journal*, Vol. 20, July 1982, pp. 900–907.